Exclusive photoproduction of excited quarkonia in ultraperipheral collisions

Cheryl Henkels[1,*] Emmanuel G. de Oliveira[1,†] Roman Pasechnik[1,2,3,‡] and Haimon Trebien[1,§]

[1]*Departamento de Física, CFM, Universidade Federal de Santa Catarina,*
C.P. 476, CEP 88.040-900 Florianópolis, Santa Catarina, Brazil
[2]*Department of Astronomy and Theoretical Physics, Lund University,*
SE-223 62 Lund, Sweden
[3]*Nuclear Physics Institute ASCR, 25068 Řež, Czech Republic*

In this paper, we discuss the exclusive photoproduction of ground and excited states of $\psi(1S, 2S)$ and $\Upsilon(1S, 2S)$ in ultraperipheral collisions (UPCs). Using the potential model in order to obtain the vector meson wave function, we find a good agreement of our calculations with data from the LHC and HERA colliders for $J/\psi(1S, 2S)$ and $\Upsilon(1S)$ in γp collisions. We extend the calculations to the nuclear target case applying them to AA UPCs with the use of the shadowing and finite coherence length effects fitted to the data. Our results are compared to the recent LHC data, in both incoherent ($J/\Psi(1S)$ at 2.76 TeV) and coherent ($J/\Psi(1S)$ at 2.76 and 5.02 TeV) processes. We also show the corresponding predictions for the excited states, in the hope that future measurements could provide more detailed information about the vector meson wave functions and nuclear effects.

I. INTRODUCTION

Phenomenology of exclusive quarkonia photoproduction processes offers very sensitive and powerful probes for the associated soft and hard QCD phenomena. In the case of bottomonia $\Upsilon(1S, 2S)$ photoproduction, the heavy quark mass m_Q provides a sufficiently hard scale for the perturbative QCD framework to be applicable for a precise description of the underlying production mechanism [1–4]. However, charmonia $\psi(1S, 2S)$ photoproduction probes predominantly nonperturbative phenomena at a semihard scale. This means that a simultaneous description of the existing charmonia and bottomonia photoproduction data is required for validation of the universality of the quarkonia production mechanism that is expected to incorporate both hard and soft QCD effects on the same footing. For a detailed review on quarkonia physics, see, e.g., Refs. [5,6] and references therein.

A notable progress in understanding of the mechanisms of heavy quarkonia elastic electro- (with large photon virtuality $Q^2 \gg 0$) and photo- (with quasireal photon

$Q^2 = 0$) production has been done over the past two decades starting from ep collisions at HERA [7–11]. More recently, the ultraperipheral pA and AA collisions (UPCs) at the LHC have provided clean experimental means for probing the real photoproduction mechanisms of heavy quarkonia in photon-Pomeron fusion with intact colliding nucleons or nuclei, thanks to low QCD backgrounds. Over the past few years, a wealth of phenomenological information on elastic (exclusive) and quasielastic $J/\psi \equiv \psi(1S)$ and $\psi' \equiv \psi(2S)$ photoproduction in UPCs has become available from the LHC measurements, in particular, from LHCb [12–14], ALICE [15–19], and CMS [20,21] experiments. Meanwhile, the existing theoretical approaches remain rather uncertain due to poorly known nonperturbative and a D-wave admixture in the corresponding S-wave quarkonia wave functions [22–24], as well as the coherence phenomena particularly relevant for photoproduction in AA UPCs [1,25–27].

A standard view on quarkonia production mechanism is encapsulated in the framework of nonrelativistic QCD (NRQCD) where one assumes a small relative intrinsic motion of the heavy (nonrelativistic) quark and antiquark, with the perfectly harmonic interaction potential (see, e.g., Refs. [4,28]). For charmonia photoproduction, nonperturbative and relativistic corrections may be significant since the mass of c quark is not large enough in order to safely rely on the perturbative QCD approach. Besides, as of tradition, the lowest-order transition amplitudes for an S-wave quarkonium $Q\bar{Q} \to V$ ($V = \psi(nS), \Upsilon(nS)$ $n = 1, 2$) is conventionally assumed to have the same form as the

*cherylhenkels@hotmail.com
†emmanuel.de.oliveira@ufsc.br
‡Roman.Pasechnik@thep.lu.se
§haimontrebien@outlook.com

lowest Fock state of the photon in the light-front (LF) (or infinite-momentum) frame, $\gamma \to Q\bar{Q}$. Such an assumption about a photonlike LF quarkonium wave function is unjustified as the corresponding rest-frame wave function necessarily has an admixture of a D-wave component whose weight cannot be established in the framework of a suitable interquark interaction potential [25]. Such an uncontrollable D-wave contribution has a considerable impact on quarkonia photoproduction observables as was recently advocated in Ref. [24].

In this work, we perform an analysis of the exclusive quarkonia photoproduction in AA UPC collisions at the LHC in the phenomenologically successful color dipole picture [29,30] (for an early analysis of diffractive charmonia photoproduction in the dipole framework, see, e.g., Refs. [1–4,31]). The main focus is the quarkonia photoproduction observables in $AA \to A + V + X$ in both the coherent ($X = A$) and incoherent ($X = A^*$ with A^* being an excited state of the nucleus) scattering regimes. Here, one of the important ingredients of the production amplitude is the LF quarkonium wave function found in the framework of potential approach going beyond the NRQCD approximation. In order to avoid an unjustified D-wave effect, one starts with a pure S-wave $Q\bar{Q} \to V$ transition in the $Q\bar{Q}$-pair rest frame as a product of spin-dependent and radial components. The radial component is found by the solution of the Schrödinger equation for a given model of the interquark interaction potential. A particularly relevant feature of the excited quarkonia states is the presence of one or several nodes in their radial wave functions [4]. These imply a possible cancellation of contributions to the photoproduction amplitude coming from the regions below and above the node position, in particular, in the $\psi' \equiv \psi(2S)$ wave function causing its relative suppression compared to the J/ψ production amplitude [32]. In the spin-dependent component, a transformation of (anti)spinor of a heavy (anti)quark Q ($\bar{Q}$) from the $Q\bar{Q}$ rest frame to the LF frame known as the Melosh transform is employed. The resulting LF quarkonium wave function has been recently validated in a detailed analysis of the S-wave quarkonia electro- and photoproduction observables at HERA in Refs. [22,23] providing a consistent estimate of the underlying theoretical uncertainties.

The paper is organized as follows. In Sec. II, we provide a brief discussion of the LF potential approach for the proton target case and present the corresponding numerical results on the energy dependence of the $\gamma p \to V p$ integrated cross section compared against all the available data from the HERA, LHC, and fixed-target experiments. In Sec. III, an analysis of coherent and incoherent quarkonia photoproduction off nuclear targets is performed and the numerical results are shown against the available LHC data on AA UPCs. Finally, concluding remarks and a summary are given in Sec. IV.

II. EXCLUSIVE PHOTOPRODUCTION OFF THE PROTON TARGET

A. $\gamma p \to V p$ cross section

Consider first the case of exclusive quarkonia photoproduction in high-energy photon-proton $\gamma p \to V p$ scattering in the rest frame of the proton target. According to the dipole picture [29,30], in the high-energy regime, both the photon and the heavy quarkonium $V = \psi(nS), \Upsilon(nS)$ ($n = 1, 2$) can be considered as color dipoles whose transverse separations are frozen during their interactions with a target nucleon. The lowest-order $Q\bar{Q}$ Fock fluctuation of the projectile quasireal photon scatters off the target nucleon at a certain impact parameter and with a fixed interquark separation. This is an elementary QCD process described through the universal dipole cross section as an eigenstate of the elastic scattering operator. The same $Q\bar{Q}$ dipole is then projected $Q\bar{Q} \to V$ to a given quarkonium state V using the corresponding LF wave function. In the nonrelativistic limit, the $Q\bar{Q}$ separation is found to be $r_V \simeq 6/M_V$, in terms of the quarkonium mass M_V [3,22]. The perturbative domain then corresponds to $r_V \lesssim r_g$ where the gluon propagation length in the nucleon $r_g \sim 0.3$ fm represents the soft scale of the process [33,34]. In the case of photoproduction, this condition is satisfied only for bottomonia, while charmonia are produced predominantly in the soft regime.

The exclusive photoproduction cross section integrated over the impact parameter of γp collisions [25]

$$\sigma^{\gamma p \to V p}(W) = \frac{1}{16\pi B}(\mathrm{Im}\mathcal{A}^{\gamma p \to V p}(W))^2 \qquad (2.1)$$

is found in terms of the forward exclusive photoproduction amplitude $\mathcal{A}(W)$, the elastic slope parameter B typically fitted to the exclusive quarkonia electroproduction data available from the HERA collider, and W is the γp center-of-mass energy. For the numerical values of the slope B, we adopt the most recent energy-dependent parametrization of the HERA data known from Ref. [23].

The forward $Q\bar{Q}$ photoproduction amplitude reads

$$\mathrm{Im}\mathcal{A}^{\gamma p \to V p}(W)$$
$$= \int_0^1 d\beta \int d^2 r_\perp \Psi_V^\dagger(\beta, r_\perp)\Psi_\gamma(\beta, r_\perp)\sigma_{q\bar{q}}(x, r_\perp),$$
$$x = \frac{M_V^2}{W^2}, \qquad (2.2)$$

where $\Psi_\gamma(\beta, r_\perp)$ is the LF wave function of a transversely polarized (quasireal) photon fluctuating into a $Q\bar{Q}$ dipole and $\Psi_V(\beta, r_\perp)$ is the LF quarkonium wave function. The transverse $Q\bar{Q}$ dipole size is $\vec{r}_\perp$, $\beta = p_Q^+/p_\gamma^+$ is the longitudinal momentum fraction of the photon momentum $p_\gamma^+ = E_\gamma + p_\gamma$ carried away by a heavy quark Q.

The universal dipole cross section describing the $Q\bar{Q}$ dipole elastic scattering off the proton target is $\sigma_{q\bar{q}}(x, r_\perp)$, where x is the standard Bjorken variable used, e.g., in diffractive Deep Inelastic Scattering (DIS) [35] and associated with the proton energy loss in the dipole-proton scattering.

In the NRQCD limit, one typically assumes an equal energy sharing between Q and $\bar{Q}$, such that the LF quarkonium wave function is approximated as $\Psi_V(\beta, r_\perp) \propto \delta(\beta - 1/2)$ [1]. Another imposed approximation is a photonlike $Q\bar{Q} \to V$ transition amplitude, with the radial wave function based upon a naive harmonic interquark potential [4,28]. In our analysis below, we go beyond these approximations following the formalism of Refs. [23,25] for the proton target, and then adopt it for the studies of quarkonia photoproduction observables in AA UPCs as done in Refs. [25,27].

B. Quarkonium wave function

A consistent computation of the LF quarkonium wave function $\Psi_V(\beta, r_\perp)$ in the infinite-momentum frame remains a challenging problem even for the lowest Fock $V \to |Q\bar{Q}\rangle$ state [25]. In this work, we follow the potential approach of Refs. [23,25] starting from the factorized wave function for a pure S-wave state in the light-cone (LC) momentum representation defined as

$$\Psi_V^{(\mu,\bar{\mu})}(\beta, \vec{p}_T) = U^{(\mu,\bar{\mu})}(\beta, \vec{p}_T)\psi_V(\beta, p_T),$$

$$U^{(\mu,\bar{\mu})}(\beta, \vec{p}_T) = \frac{1}{\sqrt{2}}\xi_Q^{\mu\dagger}\vec{\sigma}\vec{e}_V\tilde{\xi}_{\bar{Q}}^{\bar{\mu}},$$

$$\tilde{\xi}_{\bar{Q}}^{\bar{\mu}} = i\sigma_y\xi_{\bar{Q}}^{\bar{\mu}*},$$

$$\xi_Q^\mu = R(\beta, \vec{p}_T)\chi_Q^\mu,$$

$$\xi_{\bar{Q}}^{\bar{\mu}} = R(1-\beta, -\vec{p}_T)\chi_{\bar{Q}}^{\bar{\mu}} \qquad (2.3)$$

in terms of the spin-dependent and spatial (radial) parts of the vector meson wave function denoted as $U^{(\mu,\bar{\mu})}(\beta, \vec{p}_T)$ and $\psi_V(\beta, p_T)$, respectively. Here, $\vec{e}_V$ is the vector meson polarization vector, ξ_Q^μ and $\xi_{\bar{Q}}^{\bar{\mu}}$ are the heavy quark and antiquark spinors in the $Q\bar{Q}$ rest frame, respectively, related to their counterparts in the infinite momentum frame, χ_Q^μ and $\chi_{\bar{Q}}^{\bar{\mu}}$, by means of the Melosh spin transformation matrix given by [25,36]

$$R(\beta, \vec{p}_T) = \frac{-i\vec{p}_T(\vec{\sigma} \times \vec{n}) + m_Q + \beta M_V}{\sqrt{p_T^2 + (m_Q + \beta M_V)^2}}. \qquad (2.4)$$

One may assume that the corrections due to Melosh spin transformation are numerically not very relevant for a nonrelativistic $Q\bar{Q}$ system. In the case of the ground-state quarkonium states such as J/ψ, indeed, the

photoproduction cross section increases by roughly 30% only. However, in the case of excited states, the spin rotation effect is much larger and enhances $\psi(2S)$ photoproduction by about a factor 2 and 3 [22,23,25].

The spatial wave function $\psi_V(\beta, p_T)$ is typically found by using a simple Lorentz boost prescription [37] based upon the conservation of probability. Starting from the corresponding spatial wave function $\psi(p)$ in the $Q\bar{Q}$ rest frame, one writes

$$\psi_V(\beta, p_T) = \left(\frac{p_T^2 + m_Q^2}{16(\beta(1-\beta))^3}\right)^{\frac{1}{4}}\psi_V(p),$$

$$\int |\psi_V(p)|^2 d^3p = 1,$$

$$\int |\psi_V(\beta, p_T)|^2 d^2p_T d\beta = 1 \qquad (2.5)$$

in terms of the heavy quark 3-momentum $p \equiv |\vec{p}|$. This prescription, also known as the Terent'ev recipe, has been found to be quite successful in describing the HERA data on exclusive electro- and photoproduction of charmonia states in Refs. [22,23,25]. A justification of this prescription has been discussed in Ref. [38] and no significant deviation in predictions has been found between the exact calculation and the Terent'ev recipe in the phenomenologically relevant domains of the phase space.

The spatial momentum-space wave function $\psi_V(p)$ is found by a Fourier transform from the coordinate-space radial wave function $\psi(R)$ where $R \equiv |\vec{R}|$ is the interquark separation. The latter is found as a solution of the Schrödinger equation for a given interquark $Q - \bar{Q}$ interaction potential. In numerical calculations, we employ five distinct models for the interquark potential: harmonic oscillator (osc), powerlike model [39,40] (pow), Buchmuller-Tye parametrization [41] (but), Cornell potential [42,43] (cor), and logarithmic potential [44] (log). In each such parametrization of the long-distance interaction potential, the heavy quark mass m_Q ($Q = c$, b) was considered as an adjustable parameter fitted to describe the charmonia and bottomonia spectra. In the short-distance production amplitude, however, we use in numerical analysis the universal values for the charm ($m_c = 1.4$ GeV) and bottom ($m_b = 4.75$ GeV) quark masses.

C. Dipole formula for photoproduction amplitude

Using the LF quarkonia wave function in Eq. (2.3), the resulting photoproduction amplitude (2.2) can be represented in the following form [23]:

$$\text{Im}\mathcal{A}^{\gamma p \to Vp}(W) = \int_0^1 d\beta \int d^2r_\perp \left[\Sigma^{(1)}(\beta, r_\perp)\sigma_{q\bar{q}}(x, r_\perp)\right.$$

$$\left. + \Sigma^{(2)}(\beta, r_\perp)\frac{d\sigma_{q\bar{q}}(x, r_\perp)}{dr_\perp}\right], \qquad (2.6)$$

where the coefficient functions read

$$\Sigma^{(1)} = \frac{Z_Q \sqrt{N_c \alpha_{\mathrm{em}}}}{2\pi\sqrt{2}} 2K_0(m_Q r_\perp) \int \mathrm{d}p_T J_0(p_T r_\perp) \psi_V(\beta, p_T) p_T \frac{m_T m_L + m_T^2 - 2\beta(1-\beta)p_T^2}{m_L + m_T} \tag{2.7}$$

and

$$\Sigma^{(2)} = \frac{Z_Q \sqrt{N_c \alpha_{\mathrm{em}}}}{2\pi\sqrt{2}} 2K_0(m_Q r_\perp) \int \mathrm{d}p_T J_1(p_T r_\perp) \psi_V(\beta, p_T) \frac{p_T^2}{2} \frac{m_L + m_T + (1-2\beta)^2 m_T}{m_T(m_L + m_T)}.$$

Here, α_{em} is the fine structure constant, $N_c = 3$ is the number of colors in QCD, Z_Q is the electric charge of the heavy quark, $J_{0,1}$ (K_0) are the (modified) Bessel functions of the first (second) kind, respectively, p_T is the transverse momentum of the produced quarkonium state, and

$$m_T = \sqrt{m_Q^2 + p_T^2}, \qquad m_L = 2m_Q\sqrt{\beta(1-\beta)}. \tag{2.8}$$

Finally, in order to take into account the corrections due to the real part of the forward photoproduction amplitude, we included an extra factor which is the ratio of the real to imaginary parts of the scattering amplitude [25]

$$\mathcal{A}^{\gamma p \to Vp}(W)$$
$$= \mathrm{Im}\mathcal{A}^{\gamma p \to Vp}(W)\left(1 - i\frac{\pi}{2}\frac{\partial \ln \mathrm{Im}\mathcal{A}^{\gamma p \to Vp}(W)}{\partial \ln W^2}\right). \tag{2.9}$$

However, since the derivative of the imaginary part of the amplitude is sensitive only to x, we found it more convenient (see Ref. [27]) to rewrite this expression in terms of the dipole cross section,

$$\sigma_{q\bar{q}}(x, r_\perp) \Rightarrow \sigma_{q\bar{q}}(x, r_\perp)\left(1 - i\frac{\pi}{2}\frac{\partial \ln \sigma_{q\bar{q}}(x, r_\perp)}{\partial \ln W^2}\right), \tag{2.10}$$

which will be considered in further calculations.

D. Saturated dipole cross section

An essential ingredient of the photoproduction amplitude (2.6) at high energies is the universal dipole cross section $\sigma_{q\bar{q}}(x, r_\perp)$ related to the gluon distribution in the proton target. At very low x, one expects to enter a nonlinear QCD evolution regime known as saturation that constrains the maximum of the gluon density that can be achieved in the hadronic wave function (see, e.g., Refs. [45–47] and references therein). This effect is typically accounted for in phenomenological parametrizations for the dipole cross section whose saturated shape is characterized by the x-dependent saturation scale, $Q_s(x)$.

One of such simplest and most phenomenologically successful saturated models is known as the Golec-Biernat-Wustoff (GBW) [48] parametrization,

$$\sigma_{q\bar{q}}(x, r_\perp) = \sigma_0\left(1 - e^{-\frac{r_\perp^2 Q_s^2(x)}{4}}\right), \tag{2.11}$$

satisfying the renowned color transparency property of the dipole scattering, $\sigma_{q\bar{q}}(r_\perp) \propto r_\perp^2$ as $r_\perp \to 0$. Besides, we stick to the standard assumption about the quark flavor invariance of the dipole cross section in this study. In Eq. (2.11), the parametrization of the saturation scale squared in the proton target case

$$Q_s^2(x) \equiv R_0^{-2}(x) = Q_0^2\left(\frac{x_0}{x}\right)^\lambda \tag{2.12}$$

is valid at very small $x \lesssim 0.01$ only. The saturated ansatz (2.11) has given rise to a whole family of dipole models attempting in particular to incorporate the hard scale dependence of the dipole cross section via, e.g., QCD Dokshitzer-Gribov-Lipatov-Altarelli-Parisi (DGLAP)-like evolution. In the case of photoproduction, however, an effect of such a scale dependence remains minor for not very large masses of the produced states and will be safely ignored in what follows. An early fit of the HERA data for the GBW model parameters in Eq. (2.11)

$$Q_0^2 = 1 \text{ GeV}^2, \qquad x_0 = 3.04 \times 10^{-4},$$
$$\lambda = 0.288, \qquad \sigma_0 = 23.03 \text{ mb} \tag{2.13}$$

has been performed in Ref. [49], yielding a good description of a big variety of various observables in both ep and pp collisions at high energies.

Motivated by an analysis of theoretical uncertainties performed in Ref. [23], in what follows we use another parametrization from Ref. [50] known as the Kopeliovich-Schafer-Tarasov (KST) model providing a reasonably good description of the real photoproduction data available from the HERA collider. When $Q^2 \to 0$, the Bjorken variable x becomes inappropriate, such that σ_0 and R_0 in Eq. (2.11) should be replaced by functions $\bar{\sigma}_0(\hat{s})$ and $\bar{R}_0(\hat{s})$ of the

dipole-target collision center-of-frame energy squared $\hat{s} \equiv W^2$ found as follows (for more details, see Ref. [51]):

$$\bar{R}_0(\hat{s}) = 0.88 \, \text{fm} (s_0/\hat{s})^{0.14}, \quad \bar{\sigma}_0(\hat{s}) = \sigma_{\text{tot}}^{\pi p}(\hat{s}) \left(1 + \frac{3 \bar{R}_0^2(\hat{s})}{8 \langle r_{\text{ch}}^2 \rangle_\pi} \right),$$
(2.14)

respectively, where

$$\sigma_{\text{tot}}^{\pi p}(\hat{s}) = 23.6 (\hat{s}/s_0)^{0.08} \, \text{mb}, \qquad \langle r_{\text{ch}}^2 \rangle_\pi = 0.44 \, \text{fm}^2$$
(2.15)

are the total pion-proton scattering cross section and the mean pion radius squared [52]. Here, $s_0 = 1000 \, \text{GeV}^2$. The KST model is generally considered to be applicable for soft and semihard processes up to scales of $Q^2 \sim 20 \, \text{GeV}^2$ or so and, thus, particularly suitable for the predominantly soft charmonia photoproduction observables.

The effects of the skewness in the unintegrated gluon density when the gluons attached to a quark-antiquark pair carry different light-front momentum fractions $x' \ll x \ll 1$ of the proton momentum are typically accounted for by an overall multiplicative correction factor slowly dependent on gluon kinematics [53,54]. The status and the exact analytic form of the skewness correction in the dipole picture of the elastic quarkonia photoproduction are not fully understood in the literature within the kinematic ranges studied in the current analysis.

In our analysis of quarkonia photoproduction in UPCs, following Refs. [25,27], we employ only GBW and KST models described above. This is also motivated by an observation of Ref. [23] that these two models provide similar results at low x and both lead to a reasonably good description of the charmonia photoproduction data at center-of-mass energies $W \lesssim 200 \, \text{GeV}$ available from the HERA collider without any additional factors.

In fact, a detailed discussion of various theoretical uncertainties in the considered processes has been given in Ref. [23], including an analysis of the skewness correction, and we follow the same reasoning in the current work. It was shown there, in particular, that the use of skewness factor typically increases the photo- and electro-production cross section of quarkonia by a factor of 1.5 and 1.6. Besides, it was demonstrated that, omitting the skewness correction, only the KST and GBW dipole parametrizations work well against the HERA data on exclusive quarkonium electroproduction, while all other known phenomenological dipole cross sections noticeably underestimate these data. An effort to obtain a better agreement with the data in these models typically provides the main reason to include formally the skewness effects adopting only an approximate factorized expression for the skewness factor [53]. However, this is based on assumptions which may not be naturally adopted or justified for an arbitrary

process and we avoid making such assumptions in the current work. In turn, the successful use of the KST [50] and GBW [48] dipole parametrizations off the proton target motivates us to use the same approach also for nuclear targets in UPCs.

Strictly speaking, the dipole parameterizations discussed above contain only the part of the gluon density that increases at low x. At large $x > 0.01$, however, the gluon density in the target decreases approximately as $g(x) \propto (1-x)^N$ suggested by the dimensional-cutting rules [55–57], where $N \sim 5 \div 8$ depending on the hard scale of the process. A multiplication of the saturation scale squared $Q_s^2(x)$ by such a kinematical threshold factor $(1-x)^N$ is often referred to as the modified dipole approach that is known to provide a significant improvement of the Drell-Yan data description at large x (while the small-x regime is practically unaffected) [58,59] (see also Ref. [60]). Along these lines, in our numerical analysis, we supplement the dipole cross section with a factor $(1-x)^{2n_s-1}$, where n_s is the number of the active spectator quarks for the process (we adopt $n_s = 4$ in this work).

E. Numerical results for $\gamma p \to V p$ cross sections

Let us now turn to a discussion of numerical results for the integrated diffractive $\gamma p \to V p$ photoproduction cross sections (i.e., with the proton target), for $V = \psi(nS)$, $\Upsilon(nS)$, $n = 1, 2$. In Fig. 1, we present the dipole model results for $\psi(1S)$ (left panel) and $\psi(2S)$ (right panel) cross sections as functions of γp center-of-mass energy, W. In this analysis, we have used five different models for the interquark potential available from the literature and mentioned earlier. We notice that for charmonia photoproduction both dipole parametrizations, GBW and KST, discussed above in Sec. II D, give very similar results so we have chosen the GBW parametrization for the presentation purposes here. Our results are compared to the data available from H1 [8], ZEUS [10], ALICE [15], and LHCb [14] measurements as well as from the fixed-target measurements at Fermilab [61–63]. One observes that all five potentials used in our calculations give a relatively good description of the data for diffractive photoproduction of both $\psi(1S)$ and $\psi(2S)$ states in the considered energy range.

In a separate dedicated analysis, we have compared the numerical results for the integrated diffractive $\gamma p \to V p$ photoproduction cross section obtained with the original GBW model [48] discussed above and with the updated GBW fit accounting for heavy quarks [64]. We notice that the numerical difference between the results obtained with these two sets of GBW parametrizations is generally very small. Another observation is that for large values of W, the results obtained with the original GBW parameterization are somewhat closer to the data points. This is the reason why we have chosen "old" GBW fit from Ref. [48] in our current analysis.
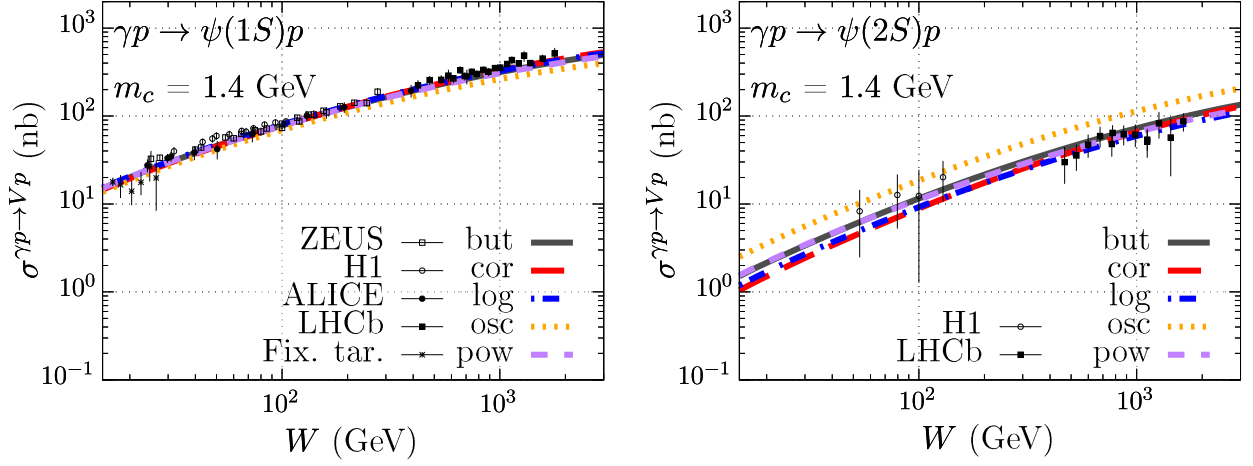
FIG. 1.   Integrated diffractive $\gamma p \to V p$ photoproduction cross section as a function of γp center-of-mass energy, W, for $V = \psi(1S)$ (left) and $V = \psi(2S)$ (right) using the GBW dipole parametrization (2.13). The results are compared with the available experimental data from H1 [8], ZEUS [10], ALICE [15], and LHCb [14] Collaborations as well as from the fixed-target experiment at Fermilab [61–63].

In Fig. 2, we show the numerical results for the integrated cross sections of diffractive $\Upsilon(1S)$ (left panel) and $\Upsilon(2S)$ (right panel) photoproduction as functions of W. In analogy to the previous figure, in our calculations of the radial wave function of the bottomonia states, we employed five different models for the $b\bar{b}$ interaction potential. The results for the ground state are confronted against the available $\Upsilon(1S)$ photoproduction data from CMS [21], H1 [7], ZEUS [9,11], and LHCb [12] Collaborations. In this figure, we have shown the results with the KST parametrization of the dipole cross section (2.14) since it provides the best description of Υ photoproduction data. It is worth noticing that all five potentials provide a comparatively good description of the available data on $\Upsilon(1S)$ in the considered energy range. This is the reason why we have used the same dipole model parametrization and the

interquark potentials for making predictions for the photoproduction cross section of the excited $\Upsilon(2S)$ state shown in the right panel. For reliable and thorough estimates of underlying theoretical uncertainties in our calculations, we refer the reader to Ref. [23] where such uncertainties have been discussed in detail.

A close inspection of Fig. 2 reveals that the difference between the γp production cross section for the ground and excited states decreases with the rise of W for all potentials. In the case of oscillator potential, for example, the result for the $\Upsilon(1S)$ is approximately 22% higher than the one for $\Upsilon(2S)$ at $W = 1000$ GeV, being the smallest difference compared to the other potentials. The observation that the oscillator potential gives relatively similar results for the ground and excited quarkonia is due to the very similar small-r dependence and magnitude of the corresponding
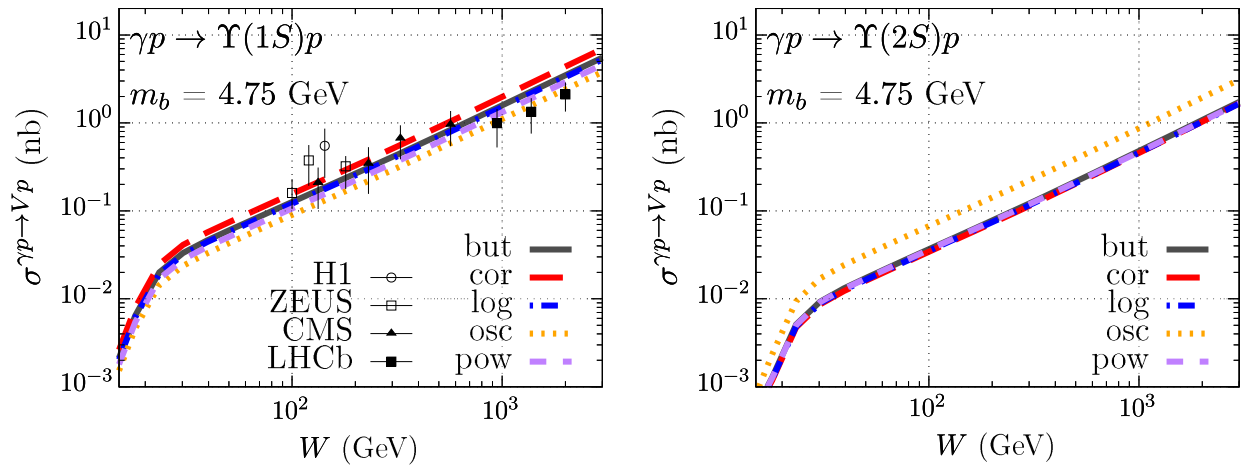

FIG. 2.   Integrated diffractive $\gamma p \to V p$ photoproduction cross section as a function of γp center-ofmass energy, W, for $V = \Upsilon(1S)$ (left) and $V = \Upsilon(2S)$ (right) using the KST dipole parametrization (2.13). The results are compared with the available experimental data from CMS [21], H1 [7], ZEUS [9,11], and LHCb [12] Collaborations.

light-front quarkonia wave functions computed with the oscillator potential (see Ref. [23] for more quantitative details). Such a dependence of the oscillator wave function is rather different compared to the other models. Since the main contribution to the integrated cross section comes from the region of small r in the radial wave function, this effect is particularly relevant for Υ states and less so for charmonia.

III. EXCLUSIVE PHOTOPRODUCTION OFF THE NUCLEUS TARGET

Let us now turn to analysis of exclusive $\psi(nS)$, $\Upsilon(nS)$, $n = 1, 2$ quarkonia photoproduction off the heavy nucleus target A relevant for the corresponding recent measurements in AA UPCs at the LHC. Here, we briefly overview an extension of the dipole model framework and the formalism of LF quarkonia wave functions to this case, as well as study the corresponding observables and confront them with all currently available data.

A. Differential $AA \to AVX$ cross section and the photon flux

In exclusive quarkonia photoproduction off the proton target considered above, the experimental data are typically provided for $\sigma_{\gamma p \to V p}$, since the photon flux, in this case, is factorized from the elastic $\gamma p \to V p$ cross section. However, such factorization does not hold in the case of a nucleus target. Indeed, a nontrivial impact parameter dependence of the photon flux becomes relevant in the AA UPCs. In the considering kinematics, the photons can only interact with the target when there is no overlap between the projectile and the target in impact parameter b space such that $b > 2R_A$, in terms of the nucleus radius R_A (for more details and review, see Ref. [65] and references therein). We also define b' as the position of the interaction point with respect to the target nucleus center, and $\vec{b}_\gamma = \vec{b}' - \vec{b}$ is the same position but with respect to the projectile nucleus.

In the center-of-mass frame of the colliding particles, the produced quarkonium state V has mass M_V and rapidity y. Also, the photon energy is labeled as ω and

$$\omega \approx \frac{M_V}{2} e^y = \frac{W^2}{2\sqrt{s}}, \tag{3.1}$$

where $\sqrt{s}$ is the projectile-target (with the projectile being a nucleon inside of an incoming nucleus and the target—a nucleon inside the target nucleus) center-of-mass energy. Of course, in numerical computations of the differential cross section, one has to take into account that the photon can be originated from each of the nuclei, which is done by incorporating $y \to -y$.

The differential cross section of quarkonia photoproduction in AA UPCs when the projectile photon is taken from one of the colliding nuclei is given in the following standard form [66]:

$$\frac{d\sigma^{AA \to AVX}}{dy} = \int d^2b \int d^2b' \omega \frac{dN_\gamma(\omega, \vec{b}_\gamma)}{d\omega d^2 b_\gamma} \frac{d\sigma^{\gamma A \to VX}(\omega, \vec{b}')}{d^2 b'},$$
$$\vec{b}_\gamma = \vec{b}' - \vec{b}, \tag{3.2}$$

where $X = A$ or A^* for the coherent and incoherent production, respectively. Provided that the photons are quasireal in the considering UPCs, i.e., $Q^2 \approx 0$, only transversely polarized photons are relevant. The photon number density in the projectile nucleus is conventionally described by the differential Weizsäcker-Williams photon flux [67,68], with a broad spectrum as given by

$$\frac{d^3 N_\gamma(\omega, \vec{b}_\gamma)}{d\omega d^2 b_\gamma} = \frac{Z^2 \alpha_{em} k^2}{\pi^2 \omega b_\gamma^2} \left[K_1^2(k) + \frac{1}{\gamma^2} K_0^2(k) \right],$$
$$k = \frac{b_\gamma \omega}{\gamma}, \tag{3.3}$$

where $\gamma = \sqrt{s}/2m_p$ is the Lorentz factor, the proton mass is given by $m_p = 0.938$ GeV, and Z is the charge of the projectile nucleus. Since at the LHC energies the Lorentz factor is large $\gamma \gg 1$ (e.g., in 2016 pPb run with $\sqrt{s} = 8.16$ TeV, $\gamma_{Pb} \approx 4350$), the second term in Eq. (3.3) can be safely omitted in practical calculations.

B. Coherent and incoherent processes

In the $\gamma A \to VX$ subprocess cross section entering in Eq. (3.2), one separates two distinct vector meson production modes. The first one, called coherent production, occurs when the nucleus target remains intact after the interaction, i.e., $X = A$. In this case, the production cross section is computed in the framework of the Good-Walker formalism [69] by averaging the color dipole interactions over all possible configurations of the projectile nucleus, thus probing the average distribution of low-x gluons in the target [70,71]. The second process called incoherent production occurs when the outgoing target nucleus does not retain the same quantum state as the incoming nucleus, i.e., it becomes an excited state A^*, which contains nucleons and nuclear fragments but no other hadrons. This process features a large gap in rapidity between the produced quarkonium and A^* system, and measures how much the scattering amplitude fluctuates between the different possible initial-state configurations [72] (for a recent detailed discussion, see, e.g., Ref. [73]).

A number of different approaches for a detailed treatment of the incoherent photo-nuclear production have been developed in the literature so far; see, e.g., Refs. [74–84].

However, an adequate simultaneous description of both coherent and incoherent processes, in the framework of the same approach, remains an open problem in the literature. Looking specifically into the incoherent case, Ref. [80] provides a reasonable description of the only available data point for J/ψ photoproduction in PbPb UPCs at 2.76 TeV from ALICE Collaboration [16], but when the same approach is used for treatment of the coherent case, it does not describe the data so well. In our work, we are primarily concerned about getting an accurate description of the coherent case (in particular, coherent J/ψ photoproduction at $\sqrt{s} = 2.76$ TeV), and then we employ the same phenomenological framework for treatment of the incoherent production as well.

Compared to the proton target case considered above, two additional effects are known to play a critical role in quarkonia photoproduction off a heavy nucleus [1,27,66]. The first one is called the color filtering, i.e., inelastic scatterings of the $Q\bar{Q}$ pair in the course of its propagation through the nucleus. The second effect is associated with the nuclear shadowing of the gluon density due to a reduction of the dipole scattering cross section off the nucleus target compared to that off the proton due to interferences. Both effects cause a reduction of quarkonia photoproduction off the nuclear target, $\gamma A \to VX$, compared to $A\sigma^{\gamma p \to Vp}$, and are effectively accounted for in our analysis below.

At high energies, the coherence (or production) length l_c defined as the lifetime of the $q\bar{q}$ fluctuation [1,85],

$$l_c = \frac{2\omega}{M_V^2}, \tag{3.4}$$

is often considered to be much larger than the nuclear radius, $l_c \gg R_A$. This guarantees a small variation of the transverse size of the dipole system and no fluctuations during the propagation process through the nucleus by means of Lorentz time dilation. In this case, a $Q\bar{Q}$ Fock fluctuation of the photon builds up long before it interacts with the nucleus target. This is called the "frozen" approximation, and the calculations are particularly simple and well known in this case.

Note, there is yet another scale called the formation length of the heavy quarkonia defined as $l_f = 2\omega/(M_{2S}^2 - M_{1S}^2)$ [1,85], which is larger than the coherence length scale. In the considered case of exclusive photoproduction, the uncertainty principle enables to resolve between J/ψ and ψ' as long as the formation length l_f is smaller than the mean inter-nucleon separation in the target nucleus. Hence, at high energies, when $l_f \gtrsim R_A$, the use of a different approach than a simple eikonalization of the photoproduction off the nucleon target is necessary.

In the frozen $l_c \to \infty$ limit, the incoherent and coherent production cross sections are found as [1,27,66]

$$\sigma^{\gamma A \to VA^*} = \int d^2b \, \frac{T_A(b)}{16\pi B} \left| \int d\beta d^2 r_\perp \Psi_V^\dagger \Psi_\gamma \sigma_{q\bar{q}}(x, r_\perp) \exp\left(-\frac{1}{2}\sigma_{q\bar{q}}(x, r_\perp) T_A(b)\right) \right|^2, \tag{3.5}$$

$$\sigma^{\gamma A \to VA} = \int d^2b \left| \int d\beta d^2 r_\perp \Psi_V^\dagger \Psi_\gamma [1 - \exp\left(-\frac{1}{2}\sigma_{q\bar{q}}(x, r_\perp) T_A(b)\right)] \right|^2, \tag{3.6}$$

respectively, where $\Psi_V = \Psi_V(\beta, r_\perp)$ and $\Psi_\gamma = \Psi_\gamma(\beta, r_\perp)$ are the LF vector meson and real photon wave functions discussed above, and $T(b)$ is the thickness function of the nucleus,

$$T(b) = \int_{-\infty}^{+\infty} dz \rho_A(b, z), \qquad \int d^2b \, T(b) = 1, \tag{3.7}$$

defined as an integral of the LC nuclear density, $\rho_A(b, z)$, over the longitudinal coordinate z at a fixed impact parameter b. In this paper, for the latter we employ the Woods-Saxon parametrization [86]

$$\rho_A(b, z) = \frac{N_A}{1 + \exp[\frac{r(b,z) - R_A}{\delta}]}, \qquad r(b, z) = \sqrt{b^2 + z^2}, \tag{3.8}$$

where $r \equiv |\vec{r}|$ is the distance from the center of the nucleus, N_A is an overall normalization factor, and the parameters $R_A = 6.62$ fm and $\delta = 0.546$ fm are taken from Ref. [87].

C. Finite coherence length

Effects due to a finite coherence length, i.e., when $l_c < R_A$, become particularly relevant at low energies W. In this case, the real photon propagates inside the nucleus target not experiencing any attenuation until it develops a $Q\bar{Q}$ fluctuation (at a short time scale t_c) which then instantly interacts with the nuclear medium. In the analysis of these dynamics, one should take into account that the produced $Q\bar{Q}$ dipole attenuates along its propagation path in the nuclear absorptive medium, whose typical mean length is roughly a half of the nuclear thickness [27].

A manifest quantum-mechanical mechanism for the propagation of such a fluctuating $Q\bar{Q}$ dipole through the nuclear medium is consistently implemented in the framework of the LC Green function approach [26]. An analytical solution for dipole Green function is known only for the simplest quadratic dependence of the dipole cross section, $\sigma_{q\bar{q}} \propto r^2$, while a generic case is treatable only numerically and is rather challenging.

Here we follow the approximation of Ref. [88] (with the explicit formulas given in Ref. [27]) in which the effect of the finite coherence length is effectively taken into account

by multiplying the infinite coherence length results (3.5) and (3.6) by a corresponding form factor as

$$\sigma^{\gamma A \to VA^*}(W^2) \Rightarrow \sigma^{\gamma A \to VA^*}(W^2)F^{\text{inc}}(W^2, l_c), \quad (3.9)$$

$$\sigma^{\gamma A \to VA}(W^2) \Rightarrow \sigma^{\gamma A \to VA}(W^2)F^{\text{coh}}(W^2, l_c) \quad (3.10)$$

for the incoherent and coherent production cross sections, respectively. In the first, incoherent case, the form factor is represented in the form explicitly normalized to the $l_c = \infty$ case as follows:

$$F^{\text{inc}}(W^2, l_c) = \int d^2 b \int_{-\infty}^{\infty} dz \rho_A(b, z)|F_1(W^2, b, z) - F_2(W^2, b, z, l_c)|^2/(\dots)|_{l_c \to \infty}. \quad (3.11)$$

Here,

$$F_1(W^2, b, z) = \exp\left(-\frac{1}{2}\sigma_{\text{VN}}(W^2)\int_z^{\infty} dz' \rho_A(b, z')\right) \quad (3.12)$$

takes into account that the incident photon fluctuates into the $Q\bar{Q}$ pair and interacts with nucleus at some point with longitudinal coordinate z, which then propagates through the nucleus and forms a vector meson. The latter then leaves without experiencing inelastic interactions. The above relation is written in terms of the energy-dependent meson-nucleon total cross section, $\sigma_{\text{VN}}(W^2)$, since the result is dominated by the $Q\bar{Q}$ dipole propagation with typical sizes relevant for $Q\bar{Q}$ projection to a particular meson state V. The second contribution in Eq. (3.11) reads

$$F_2(W^2, b, z, l_c)$$
$$= \frac{1}{2}\sigma_{\text{VN}}(W^2)\int_{-\infty}^{z} dz' \rho_A(b, z')F_1(W^2, b, z')e^{i(z'-z)/l_c}. \quad (3.13)$$

It accounts for a possibility that the photon first elastically produces a quarkonium state at a point z', $\gamma A \to VA$, which then propagates through the nucleus target without interacting till another point $z > z'$, where the last (quasielastic) scattering occurs giving rise to the final-state quarkonium, $VA \to VA^*$.

In the coherent case, the fact that the mesons produced at different longitudinal coordinates and impact parameters add up coherently simplifies the expression for the form factor compared to the previous case yielding

$$F^{\text{coh}}(W^2, l_c) = \int d^2 b \left| \int_{-\infty}^{\infty} dz \rho_A(b, z)F_1(W^2, b, z)e^{iz/l_c} \right|^2 \bigg/ (\dots)|_{l_c \to \infty}. \quad (3.14)$$

A more sophisticated Green function analysis of the coherence length effects against the recent data on quarkonia photoproduction in UPCs will be done elsewhere.

D. Gluon shadowing

At small x, the gluon density of a nucleon inside the target nucleus is suppressed compared to that of a free nucleon—the phenomenon known as the gluon (or nuclear) shadowing. In the target rest frame, this is understood as a result of the interference among incoming dipoles due to the presence of the higher Fock states of the projectile photon. The leading-order gluon shadowing correction emerges via eikonalization of the next Fock component of the photon containing the $Q\bar{Q}$ dipole plus a gluon. This

effect can be accounted for by renormalizing the dipole cross section as follows [51,66]:

$$\sigma_{q\bar{q}}(r, x) \to \sigma_{q\bar{q}}(r, x)R_g(x, \mu^2), \quad (3.15)$$

where the factor R_g represents the ratio of the gluon density inside a nucleon in the nucleus compared to the one inside the free proton, i.e.,

$$R_g(x, \mu^2) = \frac{xg_A(x, \mu^2)}{Axg_p(x, \mu^2)}. \quad (3.16)$$

In this work, we compute this factor phenomenologically using the EPPS16 nuclear parton distributions fitted to
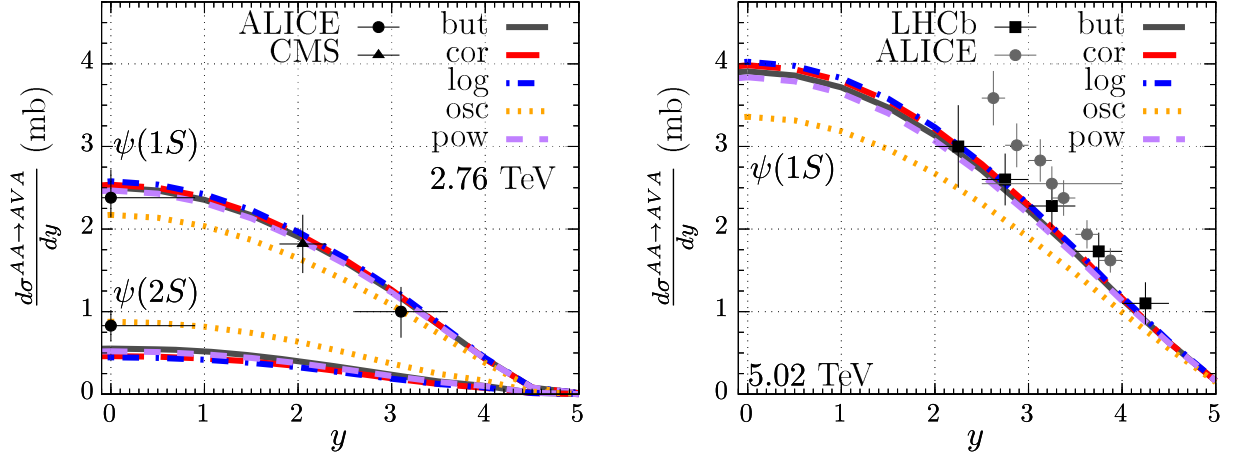
FIG. 3. Differential (in rapidity) cross section for coherent ψ photoproduction in PbPb UPCs at 2.76 TeV (left) and 5.02 TeV (right) using the GBW dipole model. The results with 2.76 TeV are compared with data from CMS [20] and ALICE [15,16] for J/ψ and from ALICE [17] for ψ', while the ones with 5.02 TeV are compared with data from ALICE [19] and preliminary results of LHCb [13].

the LHC data [89], with $\mu = M_V/2$ as the factorization scale. At this point, our calculations differ from most of previous analyses in the literature which instead have used theoretical models to predict the amount of the gluon shadowing.

E. Numerical results for $AA \rightarrow AVX$ cross sections

With all the formalism presented previously, we obtained some of the most relevant numerical results for the differential photoproduction cross sections in lead-lead collisions at the LHC energies. In Fig. 3, it is shown the differential cross sections for the coherent photoproduction of $\psi(1S)$ and $\psi(2S)$ at 2.76 TeV (left panel) and $\psi(1S)$ at 5.02 TeV (right panel) as functions of the vector meson rapidity y. In these plots, we used again the five different models for the interquark potentials and the GBW dipole model. In the left panel, we compared our results with the data from CMS [20] and ALICE [15,16] Collaborations for J/ψ and from

ALICE Collaboration [17] for ψ'. It can be noticed that our theoretical calculations describe very well the ground state production data with any of the considered interquark potentials. However, in the case of the excited state production, only the result obtained with the oscillator $c\bar{c}$ potential reaches the corresponding data within error bars. In the right panel, the results are compared with the data from the ALICE Collaboration [19] and with the preliminary data from the LHCb Collaboration [13]. In this case, our results provide a good description of the LHCb data, but fail to describe the ALICE data. We would like to point out that there is, in fact, a significant tension between these data sets themselves.

In Fig. 4, we present our results for coherent photoproduction of $\Upsilon(1S)$ (left panel) and $\Upsilon(2S)$ (right panel) at 5.02 TeV. The observable analyzed here is the differential cross section as a function of the meson rapidity calculated with the KST dipole cross section for the five distinct
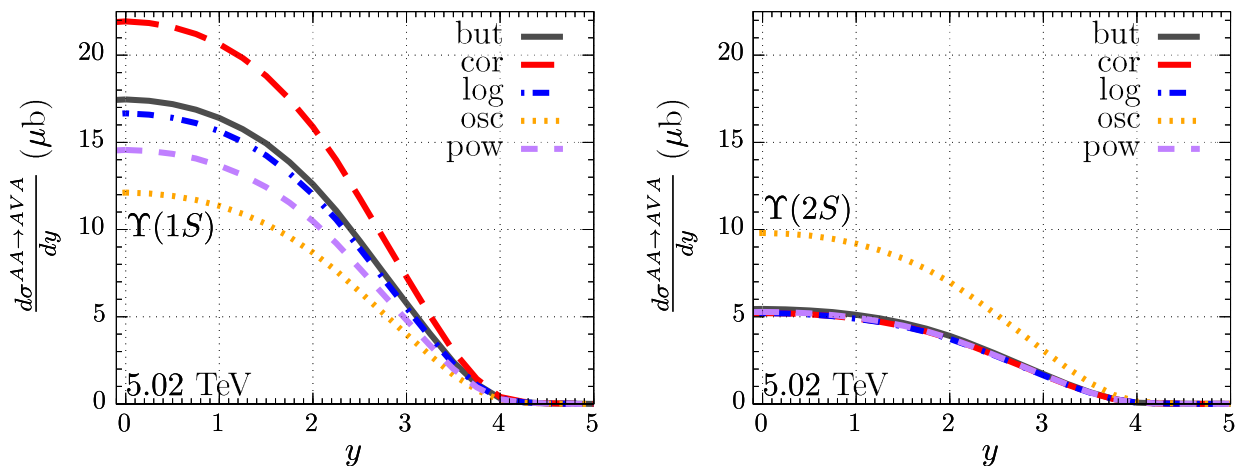

FIG. 4. Differential (in rapidity) cross section for coherent $\Upsilon(1S)$ (left) and $\Upsilon(2S)$ (right) production at 5.02 TeV in PbPb collision, using the KST dipole model.
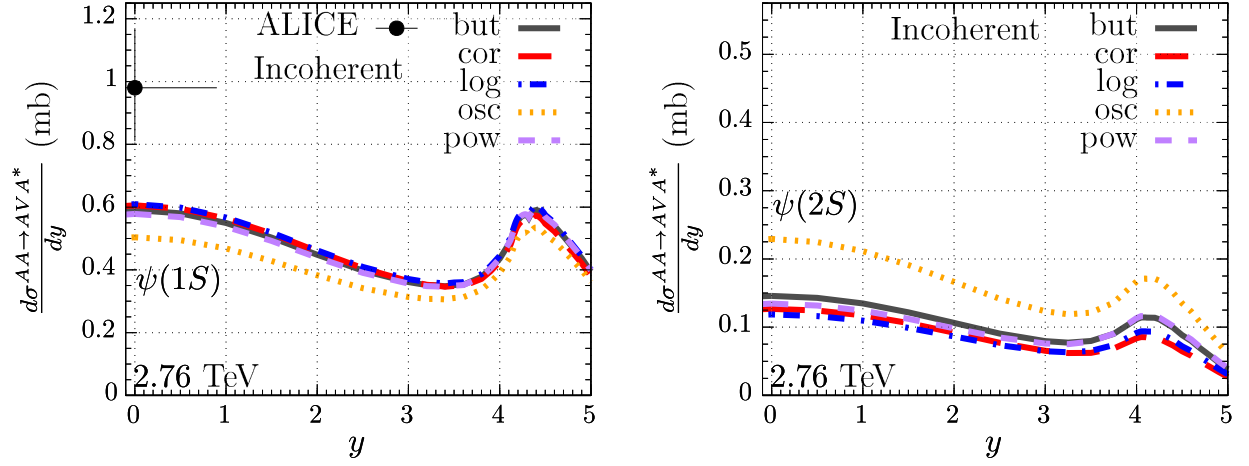
FIG. 5. Differential (in rapidity) cross section for incoherent $\psi(1S)$ (left) and $\psi(2S)$ (right) photoproduction at 2.76 TeV in PbPb UPCs. The ground state results are compared with the data from ALICE [16].

models of the $b\bar{b}$ potentials, in analogy to Fig. 3. As the reader can notice in the left panel, there is a significant spread between the results obtained with different potentials in the $\Upsilon(1S)$ production. This spread is especially pronounced at small values of the rapidity, since at large values of y the effect of the finite coherence length dominates. This is a direct consequence of the shape of the LF $\Upsilon(1S)$ wave functions that differs more from one potential to another than the other vector meson wave functions. This does not occur in the production of the excited state, however, as can be seen in the right panel. In this case, there is a good agreement between the results obtained for each potential, except for the oscillator one which gives a higher prediction.

Figure 5 shows the differential cross section for the incoherent photoproduction of $\psi(1S)$ (left panel) and $\psi(2S)$ (right panel) as a function of the meson rapidity at 2.76 TeV. These results are obtained using the GBW model and the wave functions in the potential approach and are

compared, in the case of ground state production, with the single data point from ALICE Collaboration [16]. As can be seen, the results obtained with the formalism described above do not describe the data. This means that the approach has to be improved in the case of incoherent production, and a theoretical further analysis is necessary. Nevertheless, for completeness, in Fig. 6, we show the predictions for incoherent photoproduction of $\Upsilon(1S)$ (left) and $\Upsilon(2S)$ (right) at 5.02 TeV obtained with the same formalism. As in Fig. 4, there is a spread in the predictions obtained with different interquark potentials in the case of ground state photoproduction. Such a strong sensitivity to the potential models would, in principle, enable one to set more stringent constraints on the heavy quark interaction potential once the corresponding precision data become available.

Note, the inclusion of the gluon shadowing is necessary to describe the data points for J/Ψ photoproduction in the nuclear target case. However, there is a question about the size of a possible double counting between the nuclear
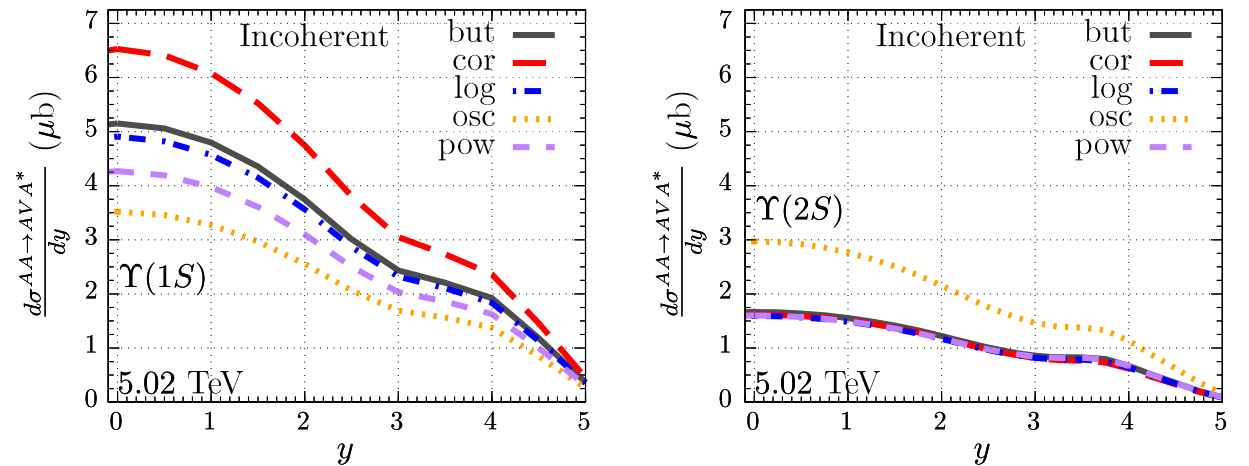

FIG. 6. Differential (in rapidity) cross section for incoherent $\Upsilon(1S)$ (left) and $\Upsilon(2S)$ (right) photoproduction at 5.02 TeV in PbPb UPCs.
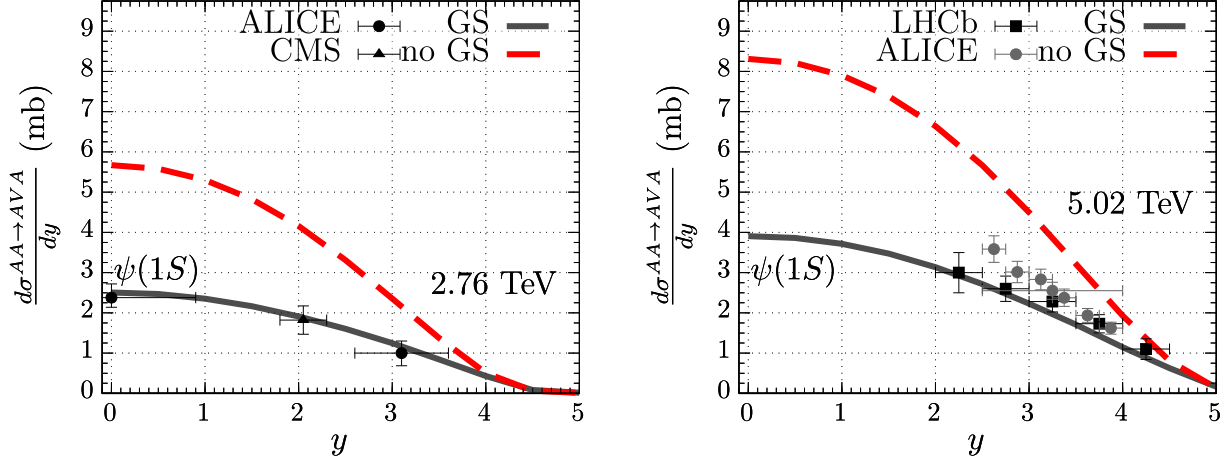
FIG. 7.   Comparison of the differential (in rapidity) cross sections of J/ψ photoproduction with and without the gluon shadowing (GS) for BUT potential versus the experimental data in PbPb UPCs at 2.76 TeV (left) and 5.02 TeV (right).

structure function and the gluon shadowing accounted for in our phenomenological approach. In order to better understand this point, in Fig. 7, we have compared the differential cross sections with and without gluon shadowing. In fact, the finite coherence length effects are relevant at large rapidities only, whereas the gluon shadowing corrections are important and closer to midrapidity. We notice that, while the Glauber corrections are included in all cases in Fig. 7, apparently they are not sufficient for the data description, while the additional gluon shadowing represents a much bigger effect relevant to achieve such a description. Thus, if there is any double counting, we expect it to be relatively small and insignificant for our first analysis.

IV. CONCLUSIONS

With the idea of reproducing what is already well known, we have described all the existing data on photoproduction of $J/\psi(1S)$, $\psi(2S)$, and $\Upsilon(1S)$ off the proton target with a good accuracy using the GBW and KST dipole models and different interquark interaction potentials for the light-front vector meson wave functions. We have also made predictions for the $\Upsilon(2S)$ photoproduction in this case, for the sake of completeness.

After establishing that the proton target case was well understood in our case, we moved to the nucleus target. In order to do so, we included the important effects of gluon shadowing and finite coherence length of the quark-antiquark dipole. So far, in the literature, the combined use of the gluon shadowing fitted to data and the interquark potential models (with Melosh spin rotation) for the quarkonia wave function has not been employed. Furthermore, no predictions for the bottomonia using the potential model were available as far as we know.

To start with, we considered the case of coherent photoproduction when the whole nucleus interacts with the photon. We achieved a good description of the $J/\psi(1S)$

and $\psi(2S)$ ALICE and CMS data sets from AA UPCs with a center-of-mass energy of 2.76 TeV. At a higher energy of 5.02 TeV, our description is consistent with the LHCb data, while there is some tension with the ALICE data. We have also made predictions for the $\Upsilon(1S)$ and $\Upsilon(2S)$ photoproduction in AA UPCs that can potentially help in determining the best interquark potential for the $b\bar{b}$ vector mesons.

In the incoherent case, we make predictions for the same four vector meson states. The only available data point (from ALICE) does not agree with our calculation. Nevertheless, we chose to show these predictions because there is in the literature a well-known difficulty of describing the incoherent production data of any type. Therefore, we have demonstrated the best description that can be achieved with the (approximate) models described in this paper and in the literature.

As a final conclusion, we would like to mention that the coherent production case can be described very well if the complete treatment of nuclear effects and vector meson light-front wave functions discussed here is employed. Regarding the incoherent case, we see a strong need for further precise measurements and a better theoretical description of the underlying physics.

[1] B. Z. Kopeliovich and B. G. Zakharov, Phys. Rev. D **44,** 3466 (1991).

[2] B. Z. Kopeliovich, J. Nemchick, N. N. Nikolaev, and B. G. Zakharov, Phys. Lett. B **324,** 469 (1994).

[3] J. Nemchik, N. N. Nikolaev, and B. G. Zakharov, Phys. Lett. B **341,** 228 (1994).

[4] J. Nemchik, N. N. Nikolaev, E. Predazzi, and B. G. Zakharov, Z. Phys. C **75,** 71 (1997).

[5] I. P. Ivanov, N. N. Nikolaev, and A. A. Savin, Phys. Part. Nucl. **37,** 1 (2006).

[6] N. Brambilla *et al.*, Eur. Phys. J. C **71,** 1534 (2011).

[7] C. Adloff *et al.* (H1 Collaboration), Phys. Lett. B **483,** 23 (2000).

[8] C. Alexa *et al.* (H1 Collaboration), Eur. Phys. J. C **73,** 2466 (2013).

[9] J. Breitweg *et al.* (ZEUS Collaboration), Phys. Lett. B **437,** 432 (1998).

[10] S. Chekanov *et al.* (ZEUS Collaboration), Eur. Phys. J. C **24,** 345 (2002).

[11] S. Chekanov *et al.* (ZEUS Collaboration), Phys. Lett. B **680,** 4 (2009).

[12] R. Aaij *et al.* (LHCb Collaboration), J. High Energy Phys. 09 (2015) 084.

[13] A. Bursche (LHCb Collaboration), Nucl. Phys. **A982,** 247 (2019).

[14] R. Aaij *et al.* (LHCb Collaboration), J. High Energy Phys. 10 (2018) 167.

[15] B. Abelev *et al.* (ALICE Collaboration), Phys. Lett. B **718,** 1273 (2013).

[16] E. Abbas *et al.* (ALICE Collaboration), Eur. Phys. J. C **73,** 2617 (2013).

[17] J. Adam *et al.* (ALICE Collaboration), Phys. Lett. B **751,** 358 (2015).

[18] E. L. Kryshen (ALICE Collaboration), Nucl. Phys. **A967,** 273 (2017).

[19] S. Acharya *et al.* (ALICE Collaboration), Phys. Lett. B **798,** 134926 (2019).

[20] V. Khachatryan *et al.* (CMS Collaboration), Phys. Lett. B **772,** 489 (2017).

[21] A. M. Sirunyan *et al.* (CMS Collaboration), Eur. Phys. J. C **79,** 277 (2019).

[22] M. Krelina, J. Nemchik, R. Pasechnik, and J. Cepila, Eur. Phys. J. C **79,** 154 (2019).

[23] J. Cepila, J. Nemchik, M. Krelina, and R. Pasechnik, Eur. Phys. J. C **79,** 495 (2019).

[24] M. Krelina, J. Nemchik, and R. Pasechnik, Eur. Phys. J. C **80,** 92 (2020).

[25] J. Hufner, Yu. P. Ivanov, B. Z. Kopeliovich, and A. V. Tarasov, Phys. Rev. D **62,** 094022 (2000).

[26] B. Z. Kopeliovich, J. Nemchik, A. Schafer, and A. V. Tarasov, Phys. Rev. C **65,** 035201 (2002).

[27] Yu. P. Ivanov, B. Z. Kopeliovich, A. V. Tarasov, and J. Hüfner, Phys. Rev. C **66,** 024903 (2002).

[28] L. Frankfurt, W. Koepf, and M. Strikman, Phys. Rev. D **54,** 3194 (1996).

[29] B. Z. Kopeliovich, L. I. Lapidus, and A. B. Zamolodchikov, Pis'ma Zh. Eksp. Teor. Fiz. **33,** 612 (1981) [JETP Lett. **33,** 595 (1981)].

[30] N. N. Nikolaev and B. G. Zakharov, Zh. Eksp. Teor. Fiz. **105,** 1117 (1994) [J. Exp. Theor. Phys. **78,** 598 (1994)].

[31] M. B. G. Ducati, M. T. Griep, and M. V. T. Machado, Phys. Rev. C **88,** 014910 (2013).

[32] J. Nemchik, Phys. Rev. D **63,** 074007 (2001).

[33] B. Z. Kopeliovich and B. Povh, J. Phys. G **30,** S999 (2004).

[34] B. Z. Kopeliovich, B. Povh, and I. Schmidt, Nucl. Phys. **A782,** 24 (2007).

[35] M. G. Ryskin, R. G. Roberts, A. D. Martin, and E. M. Levin, Z. Phys. C **76,** 231 (1997).

[36] H. J. Melosh, Phys. Rev. D **9,** 1095 (1974).

[37] M. V. Terentev, Sov. Yad. Fiz. **24,** 207 (1976) [J. Nucl. Phys. **24,** 106 (1976)].

[38] B. Z. Kopeliovich, E. Levin, I. Schmidt, and M. Siddikov, Phys. Rev. D **92,** 034023 (2015).

[39] A. Martin, Phys. Lett. **93B,** 338 (1980).

[40] N. Barik and S. N. Jena, Phys. Lett. **97B,** 265 (1980).

[41] W. Buchmuller and S. H. H. Tye, Phys. Rev. D **24,** 132 (1981).

[42] E. Eichten, K. Gottfried, T. Kinoshita, K. D. Lane, and T.-M. Yan, Phys. Rev. D **17,** 3090 (1978); **21,** 313(E) (1980).

[43] E. Eichten, K. Gottfried, T. Kinoshita, K. D. Lane, and T.-M. Yan, Phys. Rev. D **21,** 203 (1980).

[44] C. Quigg and J. L. Rosner, Phys. Lett. **71B,** 153 (1977).

[45] H. Weigert, Prog. Part. Nucl. Phys. **55,** 461 (2005).

[46] J. Jalilian-Marian and Y. V. Kovchegov, Prog. Part. Nucl. Phys. **56,** 104 (2006).

[47] F. Gelis, E. Iancu, J. Jalilian-Marian, and R. Venugopalan, Annu. Rev. Nucl. Part. Sci. **60,** 463 (2010).

[48] K. J. Golec-Biernat and M. Wusthoff, Phys. Rev. D **59,** 014017 (1998).

[49] K. J. Golec-Biernat and M. Wusthoff, Phys. Rev. D **60,** 114023 (1999).

[50] B. Z. Kopeliovich and J. Raufeisen, Lect. Notes Phys. **647,** 305 (2004).

[51] B. Z. Kopeliovich, A. Schafer, and A. V. Tarasov, Phys. Rev. D **62**, 054022 (2000).

[52] S. R. Amendolia *et al.*, Phys. Lett. **146B**, 116 (1984).

[53] A. G. Shuvaev, K. J. Golec-Biernat, A. D. Martin, and M. G. Ryskin, Phys. Rev. D **60**, 014015 (1999).

[54] A. D. Martin, M. G. Ryskin, and T. Teubner, Phys. Rev. D **62**, 014022 (2000).

[55] S. D. Drell and T.-M. Yan, Phys. Rev. Lett. **24**, 181 (1970).

[56] G. B. West, Phys. Rev. Lett. **24**, 1206 (1970).

[57] S. J. Brodsky and G. R. Farrar, Phys. Rev. Lett. **31**, 1153 (1973).

[58] B. Kopeliovich, J. Nemchik, A. Schafer, and A. Tarasov, Phys. Rev. Lett. **88**, 232303 (2002).

[59] J. Raufeisen, J.-C. Peng, and G. C. Nayak, Phys. Rev. D **66**, 034024 (2002).

[60] K. Kutak and J. Kwiecinski, Eur. Phys. J. C **29**, 521 (2003).

[61] P. L. Frabetti *et al.* (E687 Collaboration), Phys. Lett. B **316**, 197 (1993).

[62] B. H. Denby *et al.*, Phys. Rev. Lett. **52**, 795 (1984).

[63] M. E. Binkley *et al.*, Phys. Rev. Lett. **48**, 73 (1982).

[64] K. Golec-Biernat and S. Sapeta, J. High Energy Phys. 03 (2018) 102.

[65] A. J. Baltz, Phys. Rep. **458**, 1 (2008).

[66] Y. P. Ivanov, B. Z. Kopeliovich, A. V. Tarasov, and J. Hufner, AIP Conf. Proc. **660**, 283 (2003).

[67] C. F. von Weizsacker, Z. Phys. **88**, 612 (1934).

[68] E. J. Williams, Phys. Rev. **45**, 729 (1934).

[69] M. L. Good and W. D. Walker, Phys. Rev. **120**, 1857 (1960).

[70] H. I. Miettinen and J. Pumplin, Phys. Rev. D **18**, 1696 (1978).

[71] H. Kowalski, L. Motyka, and G. Watt, Phys. Rev. D **74**, 074016 (2006).

[72] A. Caldwell and H. Kowalski, Elastic and diffractive scattering, in *Proceedings, 13th International Conference,* *Blois Workshop, CERN, Geneva, Switzerland, 2009* (2009), pp. 190–192, https://inspirehep.net/literature/830497.

[73] H. Mäntysaari, arXiv:2001.10705.

[74] S. R. Klein, J. Nystrand, J. Seger, Y. Gorbunov, and J. Butterworth, Comput. Phys. Commun. **212**, 258 (2017).

[75] A. Łuszczak and W. Schäfer, Phys. Rev. C **99**, 044905 (2019).

[76] A. Łuszczak and W. Schäfer, Phys. Rev. C **97**, 024903 (2018).

[77] G. Chen, Y. Li, K. Tuchin, and J. P. Vary, Phys. Rev. C **100**, 025208 (2019).

[78] V. P. Gonçalves, M. V. T. Machado, B. Moreira, F. S. Navarra, and G. S. dos Santos, Phys. Rev. D **96**, 094027 (2017).

[79] B. Sambasivam, T. Toll, and T. Ullrich, Phys. Lett. B **803**, 135277 (2020).

[80] H. Mäntysaari and B. Schenke, Phys. Lett. B **772**, 832 (2017).

[81] J. Cepila, J. G. Contreras, and M. Krelina, Phys. Rev. C **97**, 024901 (2018).

[82] V. Guzey, M. Strikman, and M. Zhalov, Phys. Rev. C **99**, 015201 (2019).

[83] M. Ducati, F. Kopp, and M. Machado, Phys. Rev. D **96**, 054001 (2017).

[84] M. B. Gay Ducati, F. Kopp, M. Machado, and S. Martins, Phys. Rev. D **94**, 094023 (2016).

[85] S. J. Brodsky and A. H. Mueller, Phys. Lett. B **206**, 685 (1988).

[86] R. D. Woods and D. S. Saxon, Phys. Rev. **95**, 577 (1954).

[87] H. Euteneuer, J. Friedrich, and N. Vogler, Nucl. Phys. **A298**, 452 (1978).

[88] J. Hufner, B. Kopeliovich, and A. B. Zamolodchikov, Z. Phys. A **357**, 113 (1997).

[89] K. J. Eskola, P. Paakkinen, H. Paukkunen, and C. A. Salgado, Eur. Phys. J. C **77**, 163 (2017).